Journal of Power Sources 227 (2013) 284–290

Contents lists available at SciVerse ScienceDirect

Journal of Power Sources

journal homepage: www.elsevier.com/locate/jpowsour

Electrospun NiO nanofibers as high performance anode material for Li-ion batteries

Vanchiappan Aravindan [a,1], Palaniswamy Suresh Kumar [a,1], Jayaraman Sundaramurthy [a], Wong Chui Ling [a], Seeram Ramakrishna [b,*], Srinivasan Madhavi [a,c,**]

[a] Energy Research Institute @ NTU (ERI@N), Nanyang Technological University, Research Techno Plaza, 50 Nanyang Drive, Singapore 637553, Singapore
[b] Center for Nanofibers and Nanotechnology, National University of Singapore, Singapore 117576, Singapore
[c] School of Materials Science and Engineering, Nanyang Technological University, 50 Nanyang Avenue, Singapore 639798, Singapore

HIGHLIGHTS

- Electrospinning technique is used to synthesize high performance NiO nanofibers.
- NiO nanofibers rendered good cycleability and retained ~75% initial capacity after 100 cycles.
- *Ex-situ* TEM analysis confirmed the formation of Ni^0 particles during conversion reaction.

GRAPHICAL ABSTRACT

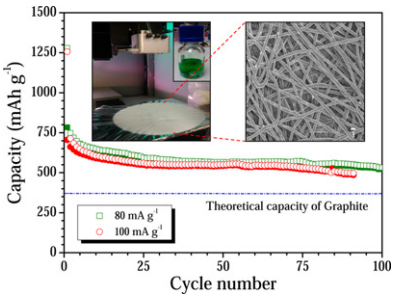

ARTICLE INFO

Article history:
Received 3 October 2012
Received in revised form
15 November 2012
Accepted 16 November 2012
Available online 27 November 2012

Keywords:
Electrospinning
Nickel oxide nanofibers
Conversion reaction
Lithium-ion battery

ABSTRACT

We report the synthesis and electrochemical performance of one dimensional NiO nanofibers by simple electrospinning technique and subsequently heat treated at 800 °C to yield single phase material. After the heat treatment, thickness and crystal size electrospun NiO is found ~1 μm and 100 nm, respectively. The electrospun nanofibers are subjected to various characterizations such as X-ray diffraction with Rietveld refinement, scanning electron microscopy and transmission electron microscopy (TEM). Half-cell assembly is used to evaluate the Li-uptake properties and found maximum reversible capacity of ~784 mA h g^{-1} at current density of 80 mA g^{-1} with operating potential of ~1.27 V *vs.* Li. The test cell rendered good cycleability and exhibits capacity retention of over 75% of reversible capacity after 100 cycles. The conversion mechanism of metallic nanoparticles (Ni^0) are validated though *ex-situ* TEM measurements. Rate performance studies are also conducted and delivered good cycling properties under such high current studies.

1. Introduction

Of late the development of high capacity anode materials are anticipated to replace the commercially available carbonaceous anodes to construct high power Li-ion power packs and its application toward hybrid electric vehicles (HEV) and electric vehicles (EV) [1–6]. Since, commercially available graphitic anodes endures several issues such as Li-platting especially at high rate operations,

* Corresponding author.
** Corresponding author. Energy Research Institute @ NTU (ERI@N), Nanyang Technological University, Research Techno Plaza, 50 Nanyang Drive, Singapore 637553, Singapore.
E-mail addresses: aravind_van@yahoo.com (V. Aravindan), seeram@nus.edu.sg (S. Ramakrishna), Madhavi@ntu.edu.sg (S. Madhavi).
[1] Contributed equally.

0378-7753/$ – see front matter © 2012 Elsevier B.V. All rights reserved.
http://dx.doi.org/10.1016/j.jpowsour.2012.11.050

less specific capacity (372 mA h g^{-1}), high processing cost etc. though exhibiting several advantages like less insertion potential (<0.25 V *vs.* Li), good chemical and electrochemical stability and eco-friendliness [7–9]. Therefore, several insertion hosts such as $Li_4Ti_5O_{12}$, $LiCrTiO_4$, anatase TiO_2, TiO_2–B, TiP_2O_7, $LiTi_2(PO_4)_3$ etc. were proposed as better alternatives for graphitic anodes however such anodes exhibiting less specific capacity (<335 mA h g^{-1}) and higher insertion potential (>1 V *vs.* Li) than graphitic anodes [10–16]. In the year 2000, Poizot et al. [17] first proposed the nanosized transition metal oxides undergo conversion reaction with lithium and provides two or three fold higher reversible capacity than graphitic anodes according to the following equilibrium, $M_xO_y + 2yLi^+ + 2ye^- \leftrightarrow xM^0 + yLi_2O$, where M belongs to transition elements such as Fe, Co, Ni, Cu etc. Since then, several transition metal oxides such as Fe_2O_3, Fe_3O_4, Co_3O_4, NiO, CuO etc., are explored as anode active material for Li-ion batteries. Among them NiO is found appealing in terms of its synthesis, high theoretical capacity (~718 mA h g^{-1} for two electron reaction), eco-friendliness and low cost. It is worth to mention that, reversible capacity and cycleability of NiO is strongly influenced by synthesis technique and its morphology [18–20]. Poor cycleability is the another main issue for such conversion type NiO anodes because of its insulating character with wide band gap of 4.3 eV and volume variation during reduction (conversion of NiO in to Ni^0) and oxidation (NiO). So far, there are several approaches have been employed to achieve high performance nanostructured NiO anodes in either native or composite form for instance, Zhang et al. [19] reviewed the electrochemical performance of various NiO nanostructures such as nanospheres, nanotubes, netlike structure, flower like structure and nanosheets. Among them, nanospeheres are exhibited specific capacity of ~510 mA h g^{-1} after 60 cycles at current density of 100 mA g^{-1}. Xia et al. [21] reported bio-templated hierarchically porous C–NiO composites from lotus pollen grains and delivered the reversible capacity of 698 mA h g^{-1} at 0.1 C rate with severe capacity fading during cycling. Synthesis of 3D-hierarchical NiO carnation is also reported and such structures capable of delivering reversible capacity of ~156 mA h g^{-1} after 50 cycles at current density of 200 mA g^{-1} by Tao et al. [22] Highly ordered mesoporous NiO by Liu et al. [23] showed the reversible capacity of ~700 mA h g^{-1} at 0.1 C rate with good cycleability. Hollow microspheres exhibited unusual electrochemical behavior with less than 85% coloumbic efficiency (reversible capacity of ~620 mA h g^{-1} at current density of 100 mA g^{-1}) is noted during cycling [24]. Mesoporous carbon encapsulated NiO rendered good cycleability of ~700 mA h g^{-1} at current density of 100 mA g^{-1} after 50 cycles [25]. Graphene–NiO hybrid composites are suggested to suppress the capacity fade by Mai et al. [26] and delivered good cycleability with capacity retention of 86% (with reversible capacity of ~721 mA h g^{-1} at current density of 100 mA g^{-1}). Solvothermal synthesized carbon-NiO microspheres are experiencing severe capacity fade during cycling and presented a reversible capacity of ~387 mA h g^{-1} after 20 cycles [27]. In this line we made an attempt to synthesize one dimensional NiO nanofiobers by electrospinning technique and evaluated as anode material in native form for first time. Since the approach of making composites with carbonaceous materials results the reduction in volumetric capacity. So far, several binary mental oxides such as TiO_2, CuO, Co_3O_4, Fe_2O_3, Nb_2O_5, carbon nanofibers are explored as possible anode active materials for Li-ion battery applications by electrospinning procedure. Guan et al. [28] first reported the synthesis of NiO nanofibers by electrospinning, however there is no work has been reported on the Li-cycleability of such nanofibers. Since, electrospinning is a very simple and versatile technique to produce single phase materials with controlled morphologies in industrial scale [29,30]. In the recent past variety of electrospun materials are developed and used for multifarious sectors particularly energy conversion and storage, dye sensitized solar cells, water splitting and purification etc. [29–31]. Among them, synthesis of electrolyte and electrolyte materials for electrochemical energy storage devices are noteworthy particularly Li-ion battery applications. In the present paper, we present the performance of electrospun NiO nanofibers as anode material for Li-ion battery applications and extensive in depth studies are conducted and presented in detail.

2. Experimental section

Simple electrospinning technique was adopted to synthesize one dimensional electrospun NiO nanofibers. In the typical synthesis procedure, Nickel acetate [$Ni(CH_3COO)_2 \cdot 4H_2O$] and N, N-dimethyl formamide (DMF, 99.8%), polyvinyl acetate (PVAc, M_W: 5×10^5) and acetic acid (99.7%) were purchased from Aldrich and used without any further purification. In a typical synthesis, sol–gel homogenous solution was prepared by mixing 2.3 g of PVAc into 20 ml DMF under constant stirring for an hour. Then, 2.1 g of Nickel acetate was introduced by wise drop in the homogenous solution followed up with 0.6 ml of acetic acid under vigorous stirring for ~12 h. The prepared sol–gel solution was then transferred into a 5 ml syringe (dia. of 11.9 mm) with 27 G stainless steel needle which has a diameter of 0.025 cm. The experiment has been carried out in a controlled electrospinning setup (ELECTROSPUNRA, Microtools Pvt. limited, and Singapore). The humidity level of the synthesis electrospinning chamber was maintained at about 35% for the whole experimental process. The distance between needle and static collector (aluminum foil) was maintained at 10 cm with an applied ac voltage of 23.5 kV and at a flow rate of 1 ml h^{-1} using a syringe pump (KDS 200). Finally, the prepared composite fibers were collected as a mat with thickness ~0.15 cm and further sintered at 800 °C for 1 h under air atmosphere to yield single phase NiO nanofibers.

Powder X-ray diffraction analysis was carried out using Bruker AXS, D8 Advance equipped with Cu Kα radiation. The observed reflections were subjected to Rietveld refinement using Topas V3 software. Morphological features and internal structure of the nanofibers were studied by field emission scanning electron microscope (FE-SEM, JEOL JFM-6340F) and transmission electron microscope (TEM, JEOL 2100F), respectively. For *ex-situ* TEM analysis, specimens were prepared under the Ar filled glove bag. The

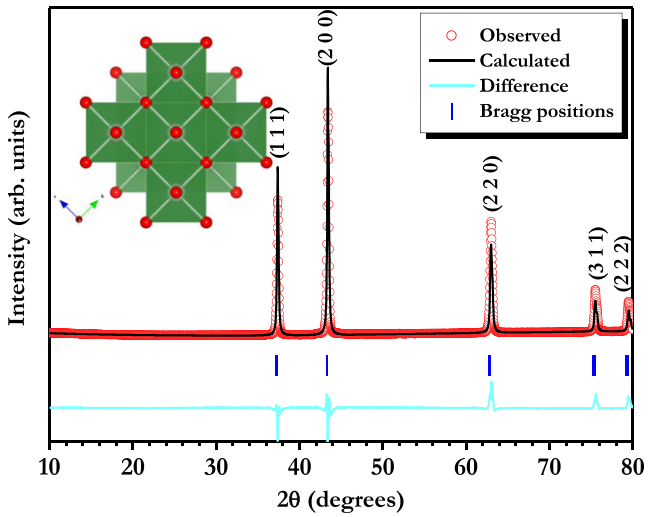

Fig. 1. Rietveld refined X-ray diffraction pattern of electrospun NiO nanofibers sintered at 800 °C for 1 h. Inset showed the crystal structure of NiO.

test cells either charged or discharged conditions were dismantled and rinsed with diethyl carbonate. The cycled active materials were carefully scratched from the current collector and transferred in to holey carbon coated Cu grid and subsequently placed in the sample holder. Then, the sample holder was fixed on the instrument with less exposure time toward atmosphere (say $<$ 10 s). Standard CR 2016 coin-cell configurations were used for all the electrochemical studies. Test electrodes were formulated with accurately weighed 10 mg of active material, 2 mg of super P, and 2 mg of conductive binder (Teflonized acetylene black, TAB) using ethanol as solvent. Then the mixture was pressed on a 200 mm^2 stainless steel mesh, which served as a current collector and dried at 60 °C for overnight before conducting coin-cell assembly in Ar filled glove box (MBraun, Germany). Microporous glass fibers (Whatman, Cat. No. 1825-047, UK) were used to separate test electrodes in coin-cell assembly and 1 M $LiPF_6$ in ethylene carbonate (EC)/di-methyl carbonate (DMC) (Selectipure SP30, Merck KGaA, Germany) was used as the electrolyte solution. Cyclic voltammograms (CV) were recorded using Solartron, 1470E and SI 1255B Impedance/gain-phase analyzer coupled with a potentiostat in two electrode configuration at slow scan rate of 0.1 mV s^{-1} between 0.005 and 3 V *vs.* Li. For the CV measurements, metallic lithium acts as both counter and reference electrode. Galvanostatic studies were performed at constant current mode using Arbin 2000 battery tester in ambient temperature conditions.

3. Result and discussion

Fig. 1 represents the Rietveld refined powder X-ray diffraction pattern of electrospun NiO nanofibers. The observed pattern clearly indicates the formation of phase pure structure of NiO nanofibers without any impurity traces or starting materials. However, difference between the observed and simulated patterns are noted which is due to the growth of NiO particulates in fibers are oriented along (1 1 1) direction. The reflections are indexed according to the face centered cubic with rhombohedral structure and $Fm\bar{3}m$ space group. The structure is commonly known as rock-salt type structure. Lattice parameter values are calculated from the refinement and found to be $a = 4.179(8)$ Å with crystallite size value of ~72 nm. The observed values are consistent with the literature (JCPDC card No. 73-1519; $a = 4.168$ Å). The color of the obtained NiO nanofibers is in green color which indicates the good stoichiometry between Ni and O, whereas non-stoichiometric compounds are appeared black in color.

Morphological features of the electrospun NiO nanofibers were investigated through FE-SEM and presented in Fig. 2 along with optical images. Fig. 2a and b clearly showed the formation of membrane like electrospun composite fibers which mainly composed of PVAc and Ni acetate. The distance between tip and Al plate collector is crucial to form Taylor cone and subsequently acquire good quality nanofibers [32]. While employing the applied voltage, precursor solution forms a conical shape in the jets from

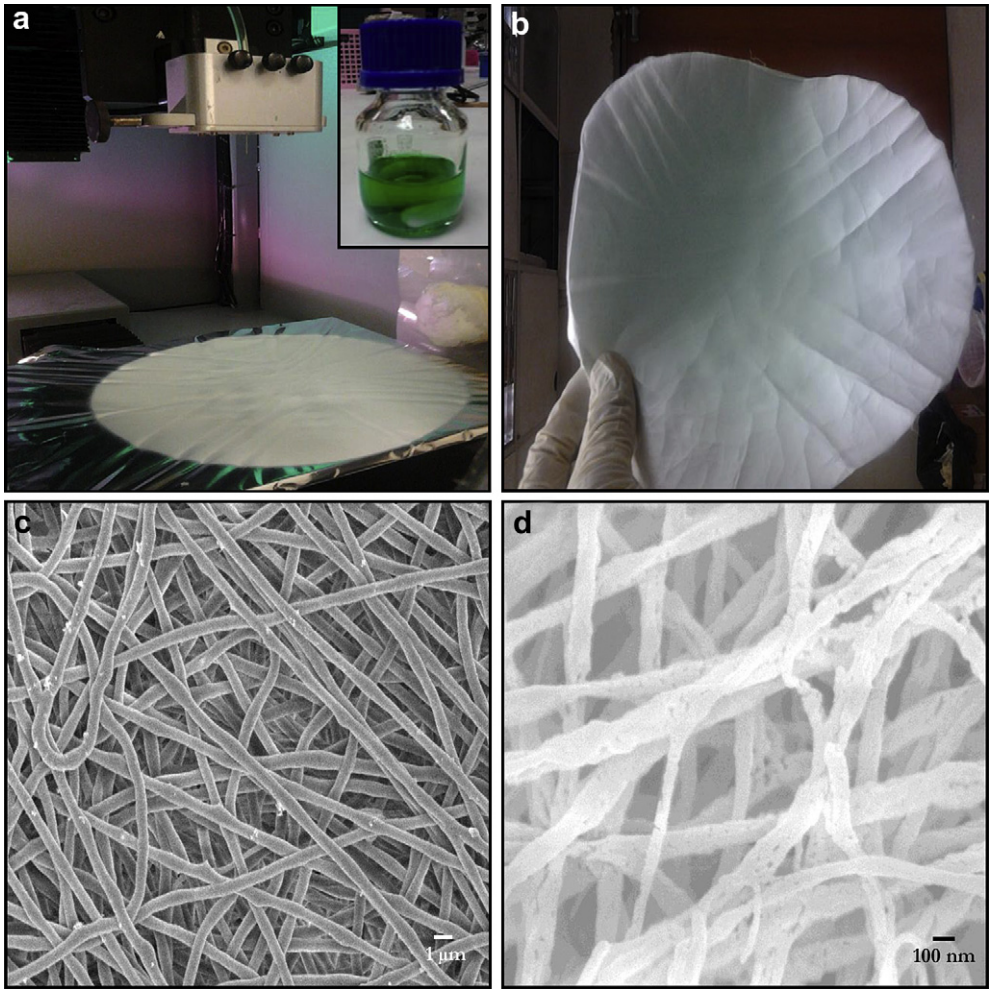

Fig. 2. (a) & (b) Photographic image of as-spun NiO nanofibers, inset showed the sol–gel precursor used for spinning, (c) scanning electron microscopy (SEM) picture of as spun NiO fibers, (d) SEM image of sintered electrospun NiO fibers at 800 °C for 1 h.

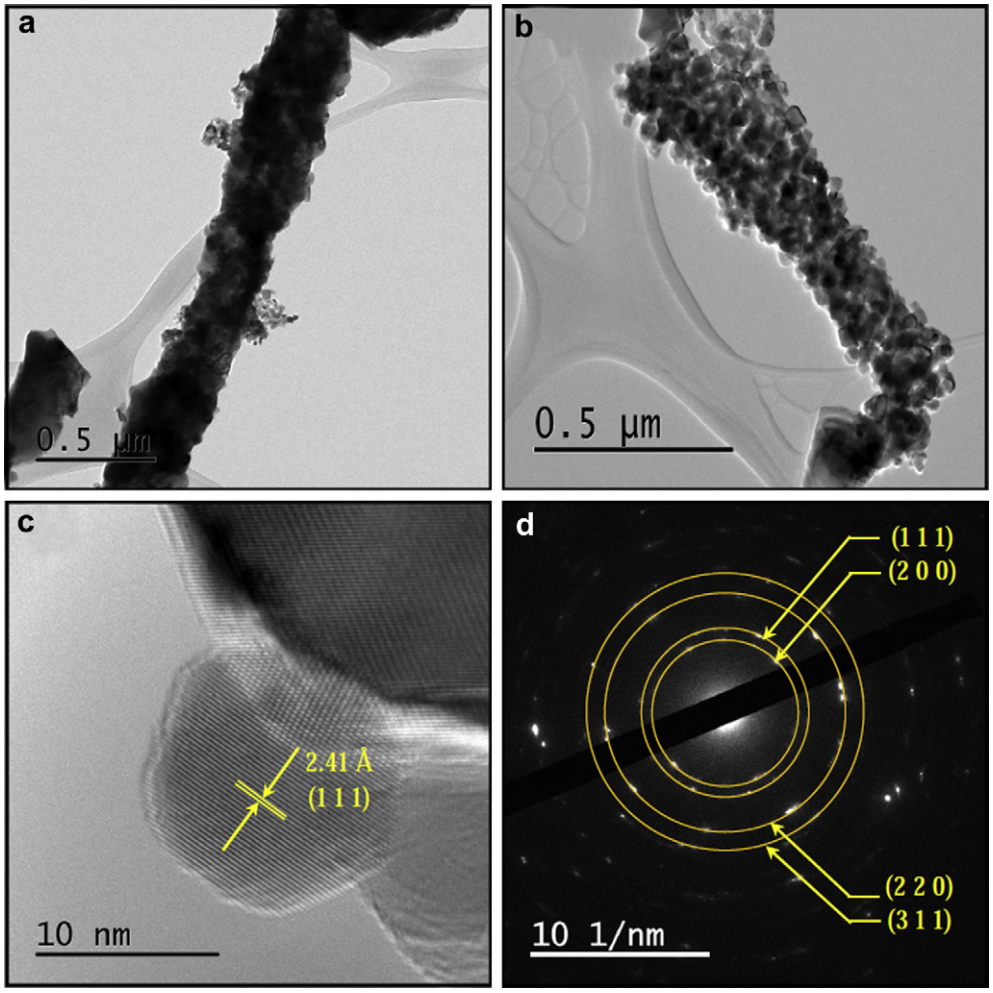

Fig. 3. (a) & (b) transmission electron microscopy (TEM) pictures of sintered NiO nanofibers, (c) high resolution-TEM image of sintered NiO nanofibers with *d* spacing of 2.41 Å along the direction (1 1 1), and (f) selected area electron diffraction (SAED) pattern of sintered electrospun NiO nanofibers with diffraction rings indexed according to the *h k l* planes.

spinneret nozzles, which is due to the electrostatic forces caused by the repulsion of surface charges and pull of external electric field. The electrostatic force overcomes surface tension of the precursor solution and Taylor cones are stretched by bending instability and deposited as a fiber over the collector. Highly interconnected, homogenous and ultra-long fibers are noted from the FE-SEM pictures (Fig. 2c) with thickness of slightly less than 1 μm. The membrane like fiber mat is harvested and sintered at 800 °C to get the desired NiO phase. Sintered as-fibers exhibited a fiberous morphology which composed of NiO nanoparticles grown along with the fiber direction during the calcination process. Thickness of such sintered fibers is found to be ~100 nm (Fig. 2d). Reduction of such fiber diameter is mainly due to the removal of organic moieties from the Ni precursors and polymer backbone as well. TEM investigations are also carried out to ensure the presence of nanoscopic NiO particles in a continuous fiberous morphology and illustrated in Fig. 3. TEM pictures with different magnifications (Fig. 3a and b) clearly illustrate the presence of nanosized particles formed as a continuous fiberous morphology. High resolution-TEM pictures clearly showed the formation of single crystalline NiO particles. The NiO nanoparticles are grown along (1 1 1) direction during the calcination process with *d* spacing of 2.41 Å (Fig. 3c). Bright spots in the selected area electron diffraction (SAED) pattern also confirmed the formation of NiO and rings are indexed to the corresponding *h k l* planes (Fig. 3d).

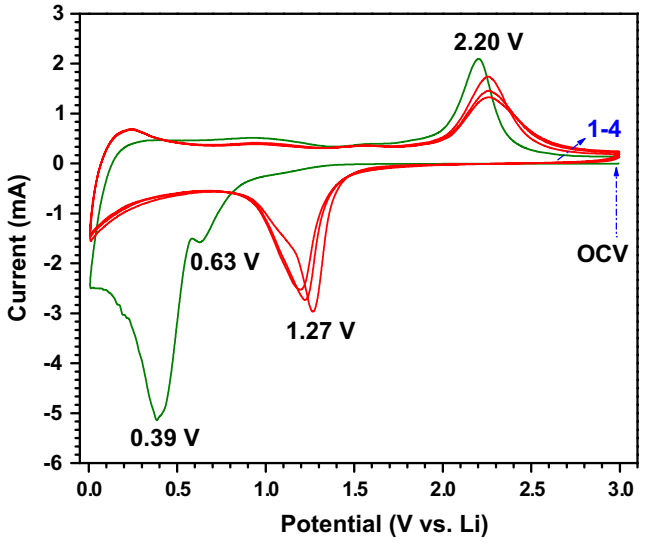

Fig. 4. Cyclic voltammetry curves of electrospun NiO nanofibers in half-cell assembly (Li/NiO nanofibers) cycled between 0.005 and 3 V *vs.* Li at scan rate of 0.1 mV s^{-1}, in which metallic lithium acts as both counter and reference electrode.

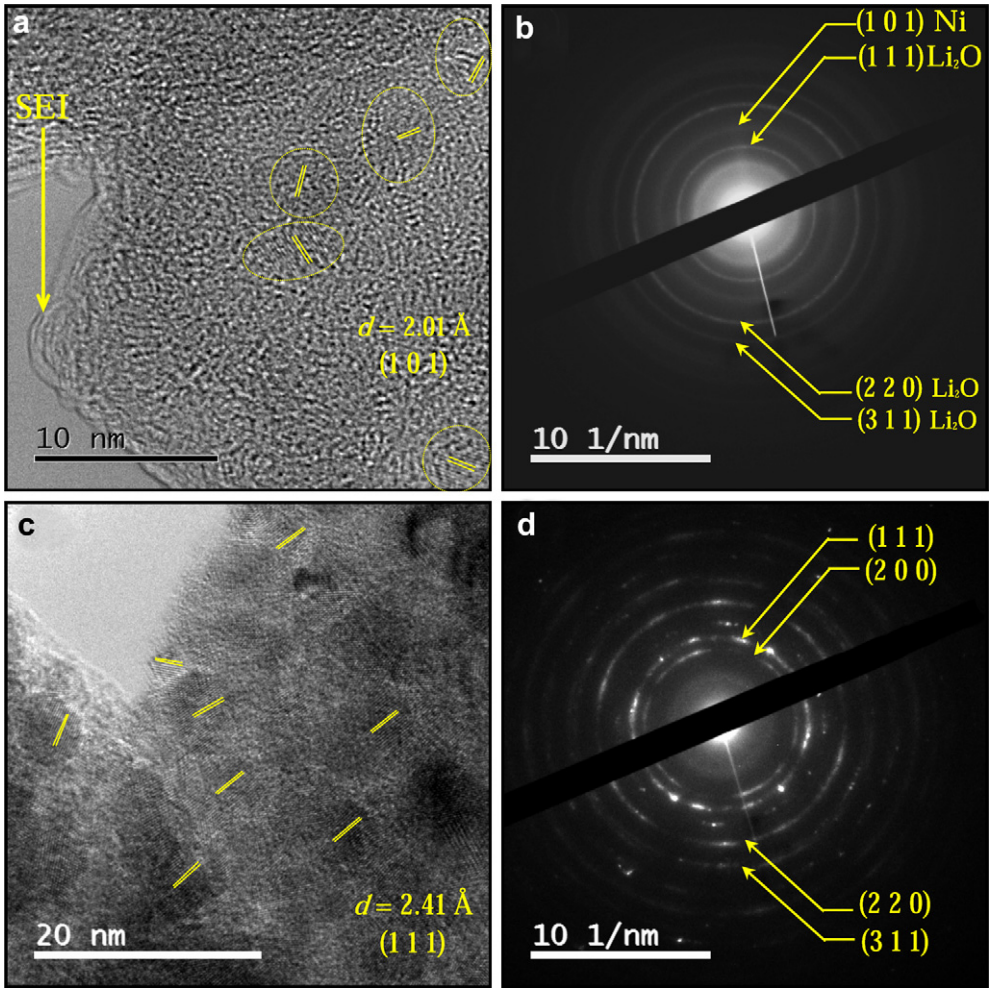

Fig. 5. (a) High resolution-transmission electron microscopy (HR-TEM) picture of electrospun NiO nanofibers at discharged state (0.005 V *vs.* Li), in which Ni^0 nanoparticles with corresponding *d* spacing is marked/given (b) selected area electron diffraction pattern (SAED) of NiO electrodes at discharged state, (c) HR-TEM image of electrospun NiO nanofibers at charged state (3 V *vs.* Li) corresponding *d* spacing is given along with orientation and (d) SAED pattern of NiO electrodes at charged state.

To understand the reaction mechanism during electrochemical charge–discharge process of electrospun NiO nanofibers, cyclic voltammetry (CV) studies was performed in half-cell configuration (Li/NiO nanofibers) between 0.005 and 3 V *vs.* Li at slow scan rate of 0.1 mV s^{-1} (Fig. 4). During first cathodic sweep, Li-insertion takes place at ~0.63 V *vs.* Li ($Li_{0.5}NiO$) and associated with electrolyte decomposition as well. The above reaction will take place in irreversible manner according to the following reaction mechanism, $NiO + 0.5\ Li^+ + 0.5\ e^- \rightarrow Li_{0.5}NiO$. Thereafter a structural destruction of above phase is occurred and evident from the strong peak potential at ~0.39 V *vs.* Li. Further, in the same region conversion of NiO in to metallic particles (Ni^0) also takes place according to the following equation $Li_{0.5}NiO + 1.5\ Li^+ + 1.5\ e^- \rightarrow Ni^0 + Li_2O$. In the anodic sweep, a broad peak potential at ~2.2 V *vs.* Li indicates the oxidation of metallic Ni^0 ($Ni^0 + Li_2O \leftrightarrow NiO$). However in the subsequent cathodic sweeps, reduction (conversion of NiO in to Ni^0) and oxidation is slightly shifted toward higher potential ca. ~1.27 V and ~2.26 V *vs.* Li, respectively in a reversible manner. The overall reaction can be written as $NiO + 2\ Li + 2\ e^- \leftrightarrow Ni^0 + Li_2O$. Capacity fading during successive cycles is noted, which is clearly evident from the reduction of net area under the CV traces.

To support the reaction mechanism described above, an *ex-situ* TEM investigations were conducted for electrospun NiO nanofibers in first charge (3 V *vs.* Li) and discharged (0.005 V *vs.* Li) states and presented in Fig. 5. The test electrodes were carefully opened and cleaned with di-ethyl carbonate before conducting the TEM analysis. According to the conversion reaction, transformation of oxides in to metal nanoparticles are distributed in the amorphous Li_2O matrix and ultrafine size hence it is too complicated to detect such particles by XRD measurements [17,18]. In the present case, ultrafine metallic Ni^0 with size of less than 5 nm are embedded in the amorphous Li_2O matrix which is finely covered with solid electrolyte interface (SEI). The presence of Ni^0 particles is clearly evident from the lattice fringes with *d* spacing of 2.01 Å, which belongs to the (1 0 1) orientation (Fig. 5a). SAED pattern (Fig. 5b) also confirm the presence of Ni^0 particles and exhibiting the diffusive rings of (1 0 1) plane along with concentric Li_2O rings [33]. Similarly, during charge process Ni^0 is oxidized in to NiO and it is clearly evident from the HR-TEM. The observed *d* spacing (2.41 Å) between the lattice fringes is exactly matching with the sintered electrospun NiO nanofibers with orientation of (1 1 1) plane. This oxidation process of Ni^0 reveals the reformation of NiO (Fig. 5c). The concentric rings in the SAED pattern in the charged states are indexed with corresponding *h k l* planes. The SAED pattern (Fig. 5d) is showing good agreement with the sintered NiO nanofibers (Fig. 3d). This *ex-situ* TEM studies well supported the reaction mechanism of NiO nanostructures during electrochemical charge-discharge process described above.

Charge–discharge studies were performed galvanostatically for electrospun NiO nanofibers in half-cell configuration between 0.005 and 3 V *vs.* Li at constant current density of 80 mA g^{-1} in ambient conditions. Typical galvanostatic charge–discharge curves are illustrated in Fig. 6. Apparent to notice the monotonous curve at ~0.7 V *vs.* Li is corresponds to the Li-insertion in to NiO matrix ($Li_{0.5}NiO$) and associated electrolyte decomposition as well in the first discharge. The long distinct plateau at ~0.6 V *vs.* Li is corresponds to the structural destruction and transformation of metallic Ni^0 as well. The cell delivered a capacity of ~1280 and ~784 mA h g^{-1} at for first discharge and charge, respectively. Observed capacity is in both charge and discharged states are higher than the theoretical capacity of NiO for two electron reaction (~718 mA h g^{-1}). The higher discharge capacity is mainly due to the polymeric film formation and some insoluble inorganic salts from the decomposition of electrolyte solution so called SEI formation and which consumes excess lithium during the first discharge [34,35]. On the other hand, slightly higher reversible capacity is noted which is mainly ascribed to the Pseudocapacitive properties of NiO [36,37]. The presence of such SEI is somewhat beneficial for the safe operation of the cell, which may prevent the unwanted side reaction with electrolyte counterpart and enables stable performance during prolonged cycling [38].

Plot of capacity *vs.* cycle number for electrospun NiO nanofibers in half-cell configuration between 0.005 and 3 V *vs.* Li at constant current density of 80 mA g^{-1} in ambient conditions is presented in Fig. 7. It is apparent to notice that, test cell experiencing more capacity fade in the initial 10 cycles and thereafter exhibits better cycleability. The capacity fading during the cycling is attributed to the inherent conducting nature of NiO phase, since the phase is lies in the wide band gap (4.3 eV) material [39]. Further, cell displayed a discharge capacity of ~583 mA h g^{-1} (1.62 mol of Li) after 100 cycles which is ~75% of its initial reversible capacity. The observed reversible capacity value is still >1.5 times higher than the theoretical capacity of graphite. Further, this is one of the best values obtained for NiO based anodes in native form compared to the previous reports described in the introduction section [18–20,40–42]. The improved performance of such anodes is mainly due to the one dimensional nanostructures prepared by electrospinning technique, which enables maximum uptake of Li during conversion reaction and good contact toward the current collectors and thereby providing good cycleability. This kind of betterment in the cycling profiles is noted for electrospun CuO nanofibers

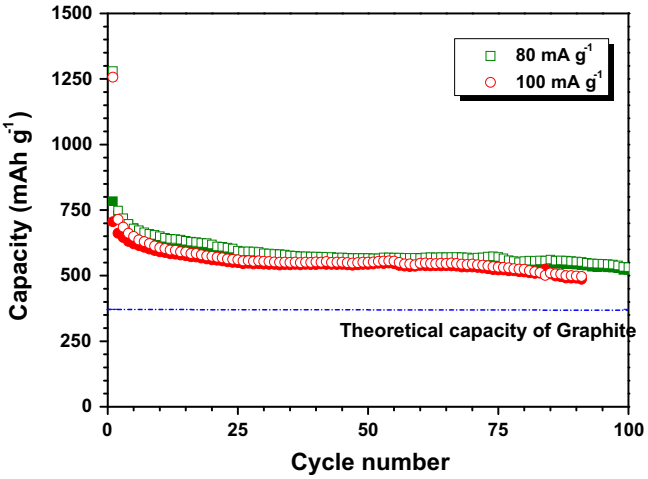

Fig. 7. Plot of capacity *vs.* cycle number for Li/electrospun NiO fibers at current densities of 80 and 100 mA g^{-1} in which filled and open symbols corresponds to the charge and discharge capacity, respectively.

reported by us recently with similar morphology [43]. In order to ensure our results, we made a duplicate cell and cycled under the same testing conditions with slightly higher current density of 100 mA g^{-1}. Apparent to notice electrospun NiO nanofibers rendered good cycleability with small deviation in the capacity values. In both cases couloumbic efficiency is found over 98% except few initial cycles which indicates good reversibility of Li-ions during conversion reaction. Further studies such as carbon coating and making composites with carbon are in progress to improve the cycleability of NiO nanofibers prepared by electrospinning.

High rate performance is one of the pre-requisite to employ as anode material in high power Li-ion power packs. Half-cell comprising electrospun NiO nanofibers was fabricated and tested with different current densities in ambient temperature conditions and given in Fig. 8. As expected, the capacity fading is noted during cycling irrespective of the current densities applied. The test cell delivered the reversible capacity of 675, 543, 409, 292 and 204 mA h g^{-1} at current densities of 0.2, 1, 2, 4 and 8 A g^{-1}, respectively with coloumbic efficiency over 98%. Lower capacity value at higher current density is presumably due to the less

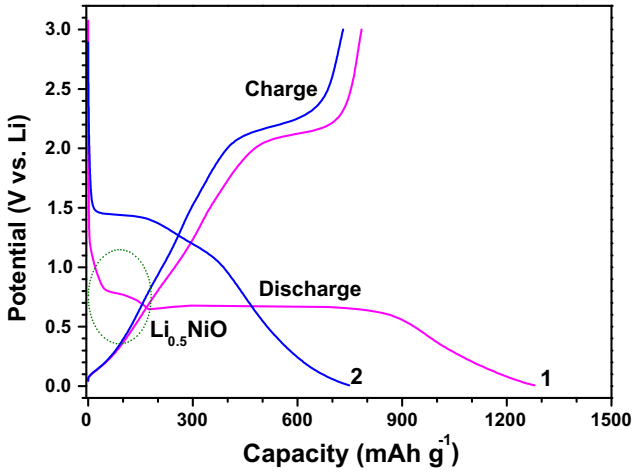

Fig. 6. Galvanostatic charge–discharge curves of electrospun NiO nanofibers in half-cell assembly cycled between 0.005 and 3 V *vs.* Li at constant current density of 80 mA g^{-1} in ambient temperature conditions. Integer represents cycle number.

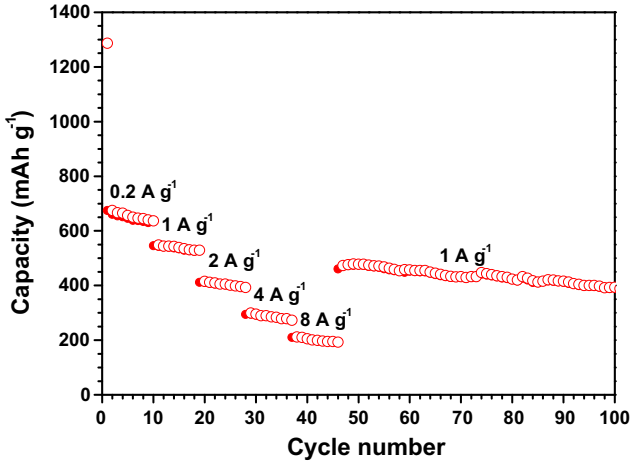

Fig. 8. Rate performance electrospun NiO nanofibers at different current densities in which filled and open symbols corresponds to charge and discharge capacity, respectively.

participation of the active material during such high current operation [44]. High current performance, particularly at 2 A g^{-1}, the cell presented the good capacity behavior (~409 mA h g^{-1}) and the obtained reversible capacity is much higher than graphitic anodes. Since such high current performance anode is anticipated for the development of high performance, high power Li-ion power packs to drive HEV and EV in neat future using such conversion type green anodes [3,45].

4. Conclusion

We successfully demonstrated the synthesis and electrochemical performance of one dimensional electrospun NiO nanofibers for first time by electrospinning technique. Formation of structure and presence of fibrous morphology was confirmed by X-ray diffraction and FE-FEM measurements, respectively. Half-cell assembly was fabricated and found maximum reversible uptake of ~1.62 mol of Li after 100 galvanostatic cycles at current density of 80 mA g^{-1} with good capacity retention of over 75% of reversible capacity. During conversion reaction, transformation of metallic Ni^0 nanoparticles in the amorphous Li_2O matrix was evidenced by *ex-situ* TEM investigations. This study clearly indicates the synthesis of high performance anode material by simple electrospinning technique and this technique can be extended for the rest of other transition metal oxides for the development of high power Li-ion power packs for HEV and EV applications.

Acknowledgment

We thank National Research foundation (NRF, Singapore) for financial support through Competitive Research Program (CRP) (Grant no. NRF-CRP4-2008-03) and Clean Energy Research Project (CERP) (Grant no. NRF-2009-EWT-CERP001-036).

References

[1] N.-S. Choi, Z. Chen, S.A. Freunberger, X. Ji, Y.-K. Sun, K. Amine, G. Yushin, L.F. Nazar, J. Cho, P.G. Bruce, Angewandte Chemie International Edition 51 (2012) 9994–10024.
[2] C.M. Hayner, X. Zhao, H.H. Kung, Annual Review of Chemical and Biomolecular Engineering 3 (2012) 445–471.
[3] E.J. Cairns, P. Albertus, Annual Review of Chemical and Biomolecular Engineering 1 (2010) 299–320.
[4] T.-H. Kim, J.-S. Park, S.K. Chang, S. Choi, J.H. Ryu, H.-K. Song, Advanced Energy Materials 2 (2012) 860–872.
[5] M.S. Whittingham, Proceedings of the IEEE 100 (2012) 1518–1534.
[6] J.B. Goodenough, Y. Kim, Chemistry of Materials 22 (2009) 587–603.
[7] Y. Nishi, The Chemical Record 1 (2001) 406–413.
[8] C.-M. Park, J.-H. Kim, H. Kim, H.-J. Sohn, Chemical Society Reviews 39 (2010) 3115–3141.
[9] M.M. Thackeray, C. Wolverton, E.D. Isaacs, Energy & Environmental Science 5 (2012) 7854–7863.
[10] V. Aravindan, W. Chuiling, S. Madhavi, Journal of Materials Chemistry 22 (2012) 16026–16031.
[11] Z. Yang, D. Choi, S. Kerisit, K.M. Rosso, D. Wang, J. Zhang, G. Graff, J. Liu, Journal of Power Sources 192 (2009) 588–598.
[12] G.-N. Zhu, Y.-G. Wang, Y.-Y. Xia, Energy & Environmental Science 5 (2012) 6652–6667.
[13] X. Su, Q. Wu, X. Zhan, J. Wu, S. Wei, Z. Guo, Journal of Materials Science 47 (2012) 2519–2534.
[14] L. Kavan, The Chemical Record 12 (2012) 131–142.
[15] S. Patoux, C. Masquelier, Chemistry of Materials 14 (2002) 5057–5068.
[16] V. Aravindan, W.C. Ling, S. Madhavi, ChemPhysChem 13 (2012) 3263–3266.
[17] P. Poizot, S. Laruelle, S. Grugeon, L. Dupont, J.M. Tarascon, Nature 407 (2000) 496–499.
[18] M.M. Rahman, S.-L. Chou, C. Zhong, J.-Z. Wang, D. Wexler, H.-K. Liu, Solid State Ionics 180 (2010) 1646–1651.
[19] G. Zhang, Y. Chen, B. Qu, L. Hu, L. Mei, D. Lei, Q. Li, L. Chen, Q. Li, T. Wang, Electrochimica Acta 80 (2012) 140–147.
[20] Y. Nuli, P. Zhang, Z. Guo, D. Wexler, H. Liu, J. Yang, J. Wang, Journal of Nanoscience and Nanotechnology 9 (2009) 1951–1955.
[21] Y. Xia, W. Zhang, Z. Xiao, H. Huang, H. Zeng, X. Chen, F. Chen, Y. Gan, X. Tao, Journal of Materials Chemistry 22 (2012) 9209–9215.
[22] L. Tao, J. Zai, K. Wang, Y. Wan, H. Zhang, C. Yu, Y. Xiao, X. Qian, RSC Advances 2 (2012) 3410–3415.
[23] H. Liu, G. Wang, J. Liu, S. Qiao, H. Ahn, Journal of Materials Chemistry 21 (2011) 3046–3052.
[24] X.H. Huang, J.P. Tu, C.Q. Zhang, F. Zhou, Electrochimica Acta 55 (2010) 8981–8985.
[25] M.-Y. Cheng, B.-J. Hwang, Journal of Power Sources 195 (2010) 4977–4983.
[26] Y.J. Mai, S.J. Shi, D. Zhang, Y. Lu, C.D. Gu, J.P. Tu, Journal of Power Sources 204 (2012) 155–161.
[27] H. Qiao, N. Wu, F. Huang, Y. Cai, Q. Wei, Materials Letters 64 (2010) 1022–1024.
[28] H. Guan, C. Shao, S. Wen, B. Chen, J. Gong, X. Yang, Inorganic Chemistry Communications 6 (2003) 1302–1303.
[29] V. Thavasi, G. Singh, S. Ramakrishna, Energy & Environmental Science 1 (2008) 205–221.
[30] S. Cavaliere, S. Subianto, I. Savych, D.J. Jones, J. Roziere, Energy & Environmental Science 4 (2011) 4761–4785.
[31] R. Sahay, P.S. Kumar, R. Sridhar, J. Sundaramurthy, J. Venugopal, S.G. Mhaisalkar, S. Ramakrishna, Journal of Materials Chemistry 22 (2012) 12953–12971.
[32] S. Ramakrishna, K. Fujihara, W.-E. Teo, C.T. Lim, Z. Ma, An Introduction To Electrospinning And Nanofibers, World Scientific, Singapore, 2005.
[33] H. Zheng, Y. Liu, S.X. Mao, J. Wang, J.Y. Huang, Scientific Reports 2 (2012) 542.1–542.4.
[34] J.S. Gnanaraj, E. Zinigrad, L. Asraf, M. Sprecher, H.E. Gottlieb, W. Geissler, M. Schmidt, D. Aurbach, Electrochemistry Communications 5 (2003) 946–951.
[35] V. Aravindan, J. Gnanaraj, S. Madhavi, H.-K. Liu, Chemistry – A European Journal 17 (2011) 14326–14346.
[36] J.-Y. Shin, D. Samuelis, J. Maier, Advanced Functional Materials 21 (2011) 3464–3472.
[37] C.T. Cherian, J. Sundaramurthy, M. Kalaivani, P. Ragupathy, P.S. Kumar, V. Thavasi, M.V. Reddy, C.H. Sow, S.G. Mhaisalkar, S. Ramakrishna, B.V.R. Chowdari, Journal of Materials Chemistry 22 (2012) 12198–12204.
[38] B. Varghese, M.V. Reddy, Z. Yanwu, C.S. Lit, T.C. Hoong, G.V. Subba Rao, B.V.R. Chowdari, A.T.S. Wee, C.T. Lim, C.-H. Sow, Chemistry of Materials 20 (2008) 3360–3367.
[39] G.A. Sawatzky, J.W. Allen, Physical Review Letters 53 (1984) 2339–2342.
[40] X. Li, A. Dhanabalan, C. Wang, Journal of Power Sources 196 (2011) 9625–9630.
[41] Y.J. Mai, J.P. Tu, X.H. Xia, C.D. Gu, X.L. Wang, Journal of Power Sources 196 (2011) 6388–6393.
[42] C. Wang, D. Wang, Q. Wang, H. Chen, Journal of Power Sources 195 (2010) 7432–7437.
[43] R. Sahay, P. Suresh Kumar, V. Aravindan, J. Sundaramurthy, W. Chui Ling, S.G. Mhaisalkar, S. Ramakrishna, S. Madhavi, The Journal of Physical Chemistry C 116 (2012) 18087–18092.
[44] K. Zaghib, J.B. Goodenough, A. Mauger, C. Julien, Journal of Power Sources 194 (2009) 1021–1023.
[45] O.K. Park, Y. Cho, S. Lee, H.-C. Yoo, H.-K. Song, J. Cho, Energy & Environmental Science 4 (2011) 1621–1633.